Material choice for the vacuum container around the LHCb VELO detector

J.F.J. van den Brand [1,2], M. Doets[1], M. Ferro-Luzzi [3], M. Kraan [1], F. Mul [2] and H. de Vries [1]

[1] NIKHEF, P.O. Box 41882, Amsterdam, The Netherlands
[2] Vrije Universiteit, 1081 HV de Boelelaan, Amsterdam, The Netherlands
[3] CERN, Geneva, Switzerland

August 28, 2003

Abstract

In an effort to minimize the amount of material, we have investigated the use of aluminium and beryllium for the detector vacuum container. Our conclusion is that the increase in cost and R&D for a design with beryllium is disproportionate with the improvement obtained.

LHCb note 2003-055

Contents

1 Introduction

The silicon detectors of the Vertex Locator are situated in a thin-walled detector vacuum container. The purpose of this container is both to separate the vacuum around the detectors from the ultra-high vacuum of the LHC accelerator, and to shield the detector and its electronics from RF signals[1], induced by the proton beams. Multiple scattering and background considerations require that the amount of material, seen by the produced particles, should be as small as possible. Therefore, the detector vacuum container must be thin and stiff, while the material used must have good electrical and heat conducting properties. Furthermore, the detectors have to overlap for acceptance coverage and alignment purposes, and it must be possible to retract the detectors such that no material is positioned at less than 27 mm from the beam axis during beam filling and tuning. This has resulted in a design with a corrugated structure as presented in the Technical Design Report (TDR) [5].

Once most subsystem technical designs were published [2, 3, 4, 5, 6], it became clear that the global amount of material in the LHCb detector was too high (approximately 0.6 radiation length X_0 and 0.2 interaction lengths λ_I on average up to RICH2, compared to the values 0.4 and 0.1 that were expected at the time of the Technical Proposal [1]). Consequently, an effort was started to minimize the amount of material in all relevant subsystems, in particular those that contributed most, *i.e.* the Outer Tracker, RICH and VELO detectors. The RICH1 detector was completely redesigned. The number of tracking stations was reduced from 9 to 3, which implied a redefinition of the tracking strategy [7]. In this process, the VELO has become an essential part of the LHCb tracking system. The number of VELO detector stations was also reduced from 25 to 21. Furthermore, we investigated the possibility to use lighter and thinner materials for the detector vacuum container, which is the subject of this note.

This note is organized as follows. We first make some practical considerations concerning the choice of material in section 2. We describe our baseline design, an aluminium container with a corrugated surface, and present results of a Finite Element Analysis (FEA) in section 3, comparing also aluminium to beryllium. We address a suggested alternative beryllium design without corrugations in section 4. A summary of our conclusions is given in section 5.

2 Practical considerations for the choice of material

Background and multiple scattering considerations strongly favor low-Z materials. Properties like vacuum tightness, strength and electrical conductivity make aluminium and beryllium the obvious candidates. Aluminium is easy to machine, it can be deformed in complicated structures, generally has good welding properties and is readily available at low cost. Pure aluminium is quite soft, but a small magnesium addition increases the strength, while welding remains relatively easy. For these reasons, aluminium was adopted for the baseline design presented in the VELO TDR. The material chosen was AlMg3, an aluminium alloy with 3% Mg that is widely available.

[1]The detector vacuum container is sometimes referred to as the 'RF box'.

Material	AlMg3	Beryllium SR-200
Young modulus	70 GPa	303 GPa
Shear modulus	27.3 GPa	113.9 GPa
Yield strength	∼80 MPa (annealed)	∼300 MPa

Table 1: *Material properties used in this study.*

The possibility to use beryllium was also investigated. Beryllium has the advantage of being lighter and stiffer. However, handling this material is difficult, as well as pressing it into a designed shape. Machining can easily damage this low-ductility material. Furthermore, welding is not simple: autogenic welding is almost impossible and the only solution is to use filler materials. Laser welding seems to offer better prospects, but so far only small-size components have been produced. Furthermore, machining involves severe safety issues and, in practice, can only be done at specific factories.

A possibility may be to machine the complete structure from solid beryllium block material. A rough estimate indicated that the price of the beryllium block alone (*i.e.* without machining it to the finished geometry detailed in the drawing) which would be needed to make a part of this size, would be in excess of 150 kUS$. Machining costs will be in addition to that. The fact that the container needs to be vacuum tight is potentially an important consideration which will affect the manufacturing costs, and the unit price was estimated to be approximately 500 kUS$ per container (including spares, at least four containers are needed). An alternative may be machining the sides of the container from individual plates of solid beryllium and then joining them together. However, the welding is considered to be risky: during welding the crystal structure changes and the requirement for the structure to be vacuum tight might increase the price. Note that brazing is not an ideal joining process for UHV applications, although it has been used in several UHV applications such as the experimental beam pipes for LEP, where however simple cylindrical pipes were used.

A detector vacuum container *without corrugations* might render the fabrication with beryllium more realistic and more affordable, the hope being that folding/bending of beryllium sheets might be easier than pressing them into a complex shape. This has motivated a study in which we have investigated the VELO performance losses for such a design and the thickness that would be required in order to make it a viable solution (see section 4).

3 The corrugated detector vacuum container

To fulfill the requirements mentioned in the introduction, a detector vacuum container equipped with corrugated foils was designed as depicted in Fig. 1. The corrugated structure of the top foil was determined by the demand to limit the amount of material, seen by the detected particles, and by the requirement that the silicon sensors should partly overlap. Furthermore, the corrugations considerably contribute to the stiffness of the vacuum container.

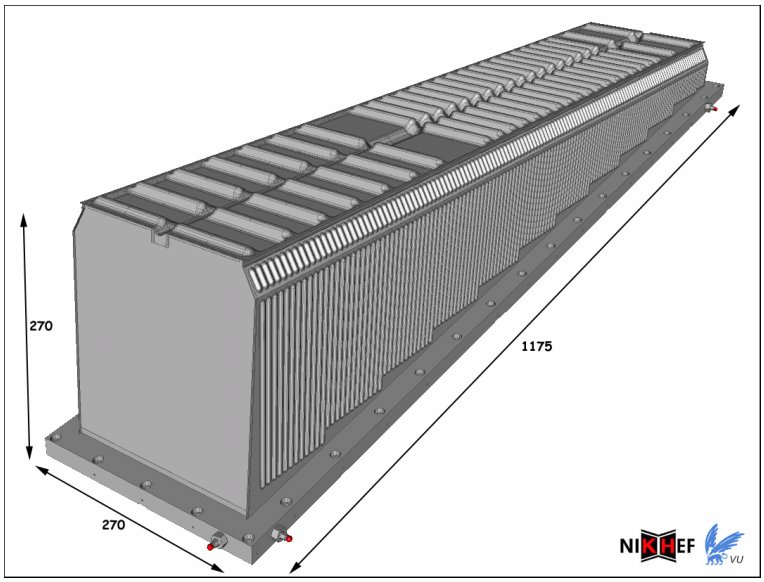

Figure 1: *The detector vacuum container with corrugated foils.*

Important aspects to consider are the maximum displacements of and maximum stresses in the foil due to pressure differences across the foil. Displacements at pressure differences which the foil will be subject to must be taken into account in the tolerances between the foil and the silicon sensors. The smaller the displacement, the closer to the beam the silicon sensors can be placed, which gives a better vertexing performance. The maximum stress in the foil needs to be known in order to estimate at what pressure difference plastic deformation will occur, a parameter that strongly influences the design of the vacuum system. To address these issues, FEA calculations have been performed. The material properties used in these calculations are given in Table 1.

In what follows, the maximum tolerable pressure difference is defined as the pressure difference at which the calculated stresses in the container reach the yield strength. No safety factor is applied. Below (above) this value, deformations are expected to be (in)elastic.

The FEA results for the displacement and the stresses for a pressure difference of 15 mbar on a 0.25 mm thick AlMg3 foil are shown in Figs. 2 and 3, respectively. The FEA were performed for both signs of the applied pressure difference. Since similar results are obtained for both signs, we present only the results for the case with a pressure which is larger on the side of the silicon detector vacuum.

Figure 4 shows the minimal thickness for which no plastic deformation occurs for an AlMg3 foil as a function of the pressure difference over the foil. An aluminium foil of $\sim$0.25 mm thickness is a reasonable compromise between requirements on the mechanical properties and the physics-driven needs. The foil is expected to withstand a pressure difference of $\sim$ 15 mbar without plastic deformation. Note that such a foil would be already the main contributor to the degradation of the VELO impact parameter resolution and give one of the largest single-item contributions to the amount of material traversed by particles before reaching the LHCb calorimeter (about 9% of a radiation length [8]).

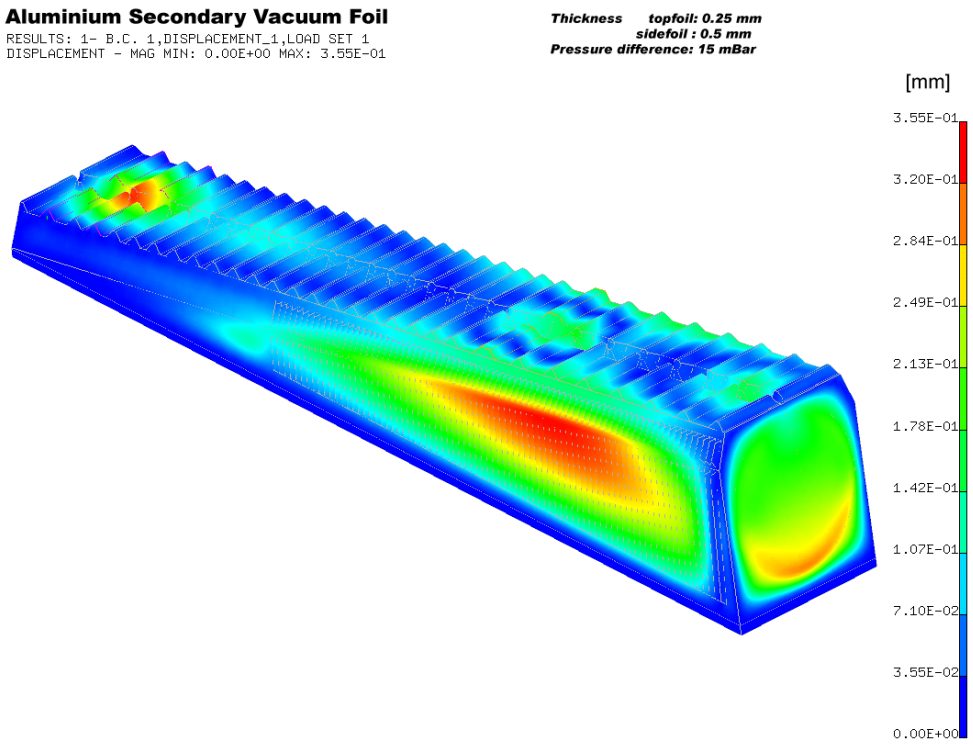

Figure 2: *Deformation of a detector vacuum container made from aluminium (thickness 0.25 mm for the top foil, 0.50 mm for the sides) at a pressure difference of 15 mbar. The maximum displacement amounts to 0.36 mm.*

Having a container that can sustain a pressure difference of 1 atmosphere would present considerable advantages in terms of handling and complexity of the vacuum system. Therefore, the minimum thickness needed to achieve this was also calculated. The calculations show that a foil thickness of about 5 mm (without any safety factor) would be necessary, which is unacceptably large.

Beryllium, being stiffer than aluminium, can withstand a higher pressure difference for the same thickness (thus, with approximately 4 times less radiation lengths and the same number of nuclear interaction lengths). In Figs. 5 and 6 the results of the deformation and stress calculations are shown for a box with 1 mm thick beryllium foil and a pressure difference of 1000 mbar (the side walls were 2 mm thick). One concludes that an atmospheric pressure difference would lead to unacceptably high stresses for a foil thickness of 1 mm (corresponding to 0.25 mm aluminium in terms of radiation lengths).

Fig. 7 shows the maximum stress in the beryllium container as a function of the pressure difference applied for a 1 mm wall thickness. The maximum tolerable pressure is expected to be between 750 and 850 mbar, taking into account some uncertainty in the yield strength. As a consequence, and without adding any safety factor, we estimate that such a beryllium container (if it can be fabricated) would need to be made with a wall of at least 1.3 mm thickness to sustain 1000 mbar. In practice, a test at a pressure 1.25 times the design pressure would have to be passed. Furthermore, such a thickness

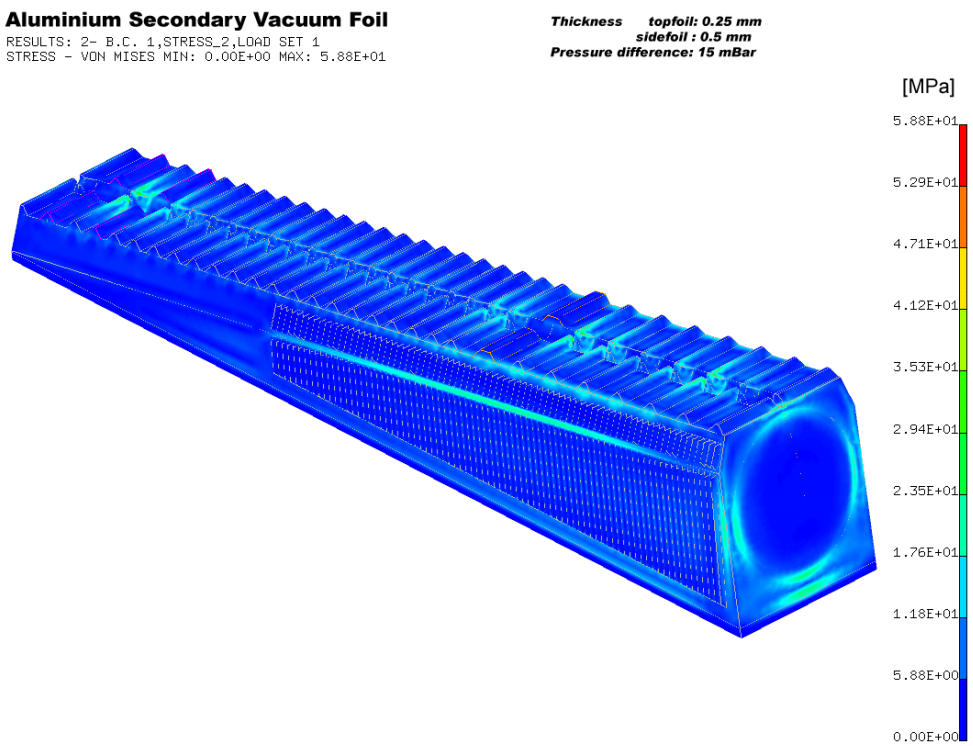

Figure 3: *Stresses in a detector vacuum container made from aluminium (thickness 0.25 mm for the top foil, 0.50 mm for the sides) at a pressure difference of 15 mbar. The maximum stress amounts to 60 MPa.*

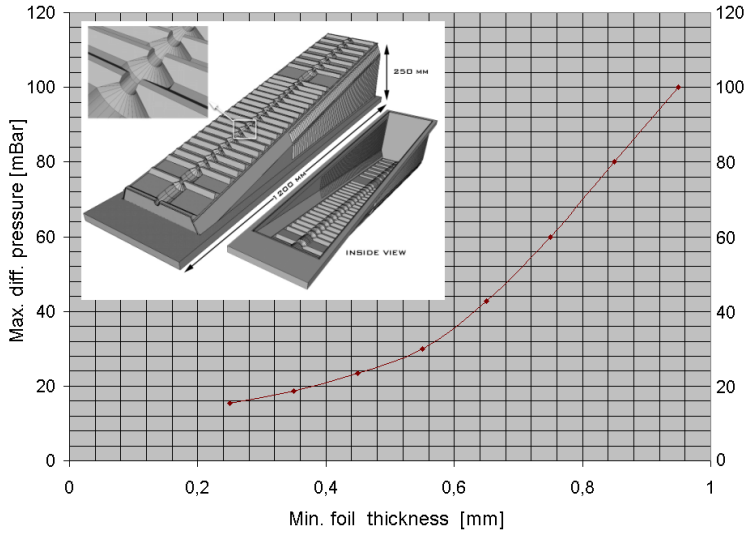

Figure 4: *FEA results that show the minimal thickness required to prevent plastic deformation versus pressure difference for the corrugated aluminium structure shown in the insert.*

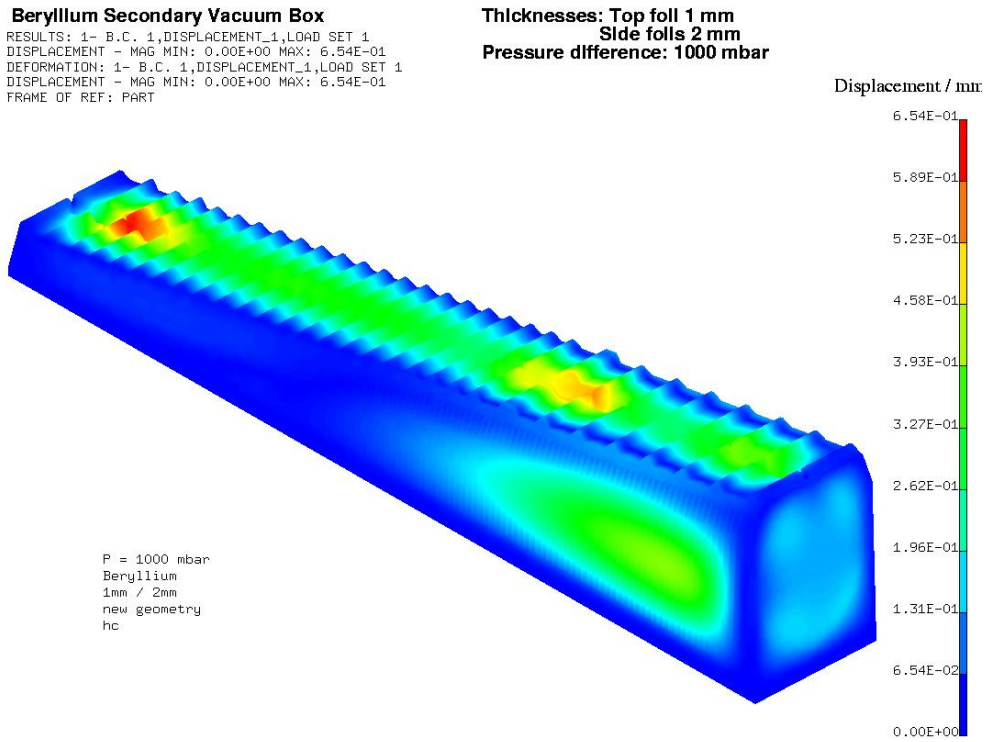

Figure 5: *Deformation of a detector vacuum container made from beryllium (thickness 1 mm for the top foil, 2 mm for the sides) at a pressure difference of 1000 mbar. The maximum displacement amounts to 0.6 mm.*

would render more difficult the task of bringing the sensitive area of the silicon detectors as close as possible to the nominal beam line.

FEA calculations were also performed for a 0.25 mm beryllium foil. However, it is doubtful that such a container can be fabricated at an affordable price. Next, we discuss an alternative design without corrugations.

4 Alternative design without corrugations

An effort was made to adapt the detector vacuum container design (and sensor design) to the fabrication constraints imposed by the beryllium option, namely a design in which the container consists of folded sheets only (without deformations)[2] as shown in Fig. 8. In this design all corrugations have been removed. Hence, there is no overlap between opposite detector halves. We remind that this overlap is an important feature of the baseline design in that it provides a close-to-perfect acceptance coverage and facilitates tracking-based relative alignment of the two halves. In such a 'flat foil' design, the acceptance losses must be reduced by shifting the gap between the opposite halves away from the mid-plane. The suggested shapes of the silicon sensors and foil boundary are sketched in

[2]The problem is actually not as simple as that: the approach ignores the problem of joining the four side walls to the side which faces the beam. One would probably again need welding or brazing.

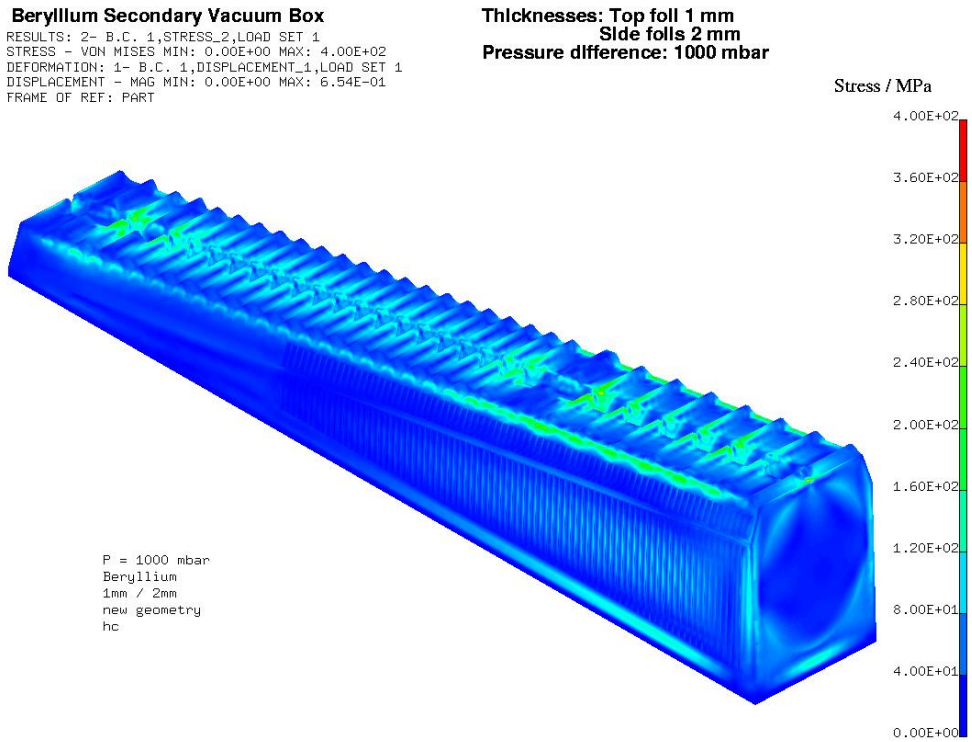

Figure 6: *Stresses in a detector vacuum container made from beryllium (thickness 1 mm for the top foil, 2 mm for the sides) for 1000 mbar pressure difference. The maximum stress amounts to 400 MPa.*

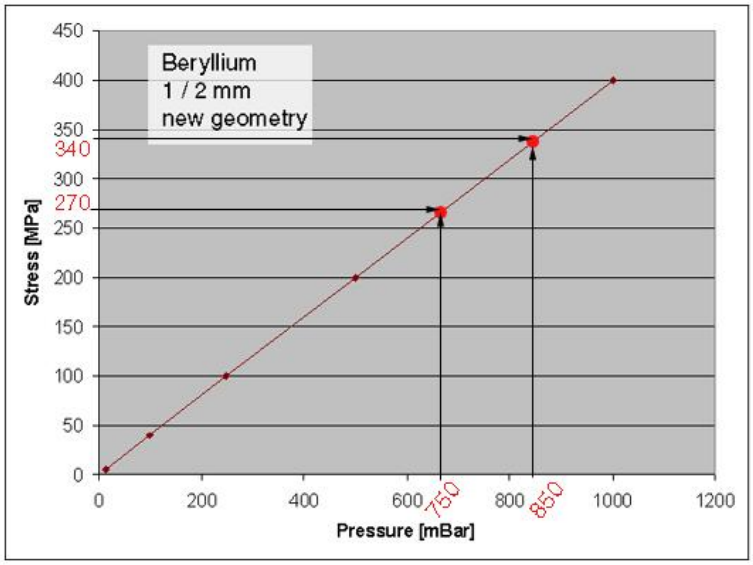

Figure 7: *FEA results that show the maximum stress in a 1 mm/2 mm beryllium container as a function of applied pressure difference.*

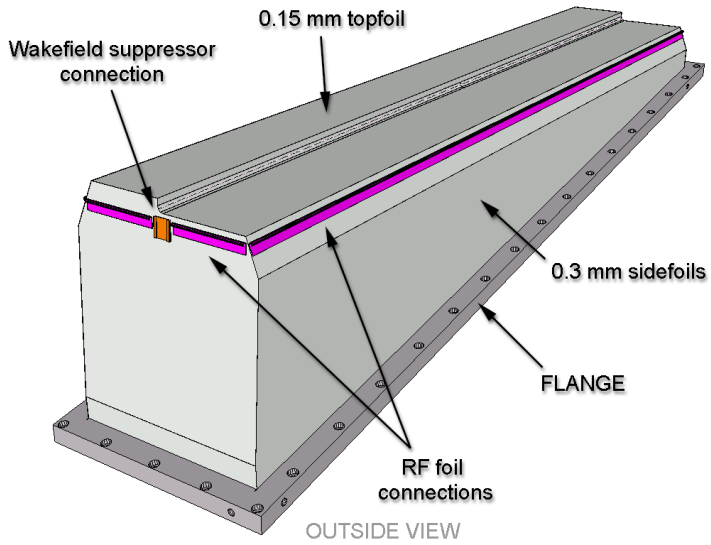

Figure 8: *A design for the detector vacuum container with a flat surface.*

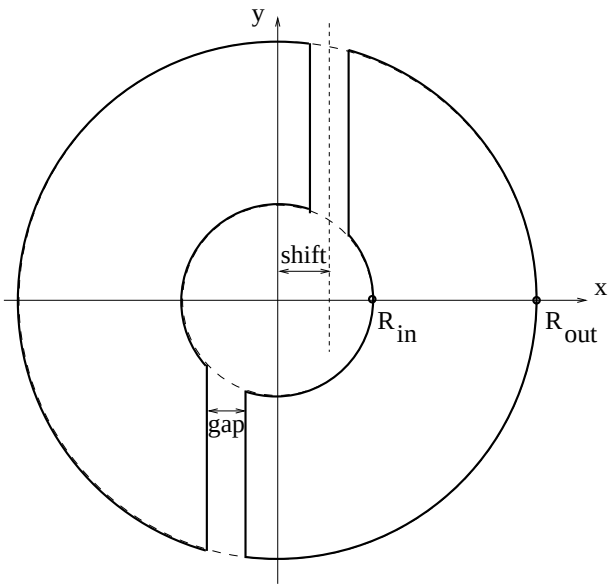

Figure 9: *Sketch of the proposed flat foil design with a gap between two opposite silicon sensors shifted away from the mid-plane. The sketch shows the active area of the sensors.*

Fig. 9. In subsection 4.1 we present the results of a study for this alternative design, in which we looked at the acceptance coverage losses and the amount of material seen by particle tracks relative to the baseline 'corrugated foil' design. In subsection 4.2 we address the mechanical properties of such a detector vacuum container made out of beryllium.

4.1 Performance studies of the flat foil design

The flat foil design sketched in Fig. 9 offers the following advantages:

- fabrication with beryllium becomes much more accessible,
- the RF shield geometry is simpler, and so is the material distribution,
- the z positions of the silicon modules are totally decoupled from the RF shield geometry,
- the number of tracks crossing the two opposite detector halves is large.

However, a number of questions have been raised, the most important ones being:

- acceptance loss: what is the probability that an interesting B-meson event is lost because of the reduced acceptance coverage ?
- what is the gain or loss in amount of material traversed by particles ?

4.1.1 Acceptance loss

We have estimated the loss in acceptance coverage due to the missing overlap by recalculating all hits in the VELO from a $B \to \pi^+\pi^-$ sample generated with SICB. The true momentum vector of the particles at their creation was used to fabricate fictitious straight tracks (no multiple scattering). Subsequently, all (x, y) hit positions at the sensor planes were found and only those falling within the sensitive area of the silicon sensors depicted in Fig. 9 were retained. A track was considered to be lost if it did not produce at least 3 pairs of hits (a pair meaning that both the r- and ϕ-sensors of one module have been hit). The losses were calculated relative to the baseline design (corrugated foil) that was used in the SICB simulation.

Fig. 10 shows (left side) the number of tracks lost due to the acceptance gap as a function of pseudo-rapidity η. The distribution is given for two extreme cases: no shift of the gap (dashed line) and with a maximum shift (6.5 mm in this case) of the gap (solid line). For these studies a gap of 3 mm was assumed between the sensitive areas of the silicon detectors, which is somewhat optimistic given that the current sensor design exhibits a 1 mm broad inactive guard ring on the wafers (leaving just a 1 mm gap for the two foils and tolerances). The inner and outer radii of the sensitive areas were set as in the TDR, namely $R_{\rm in} = 8$ mm and $R_{\rm out} = 42$ mm. The figure also shows (right side) the total fractional loss as a function of the gap shift from the mid-plane, relative to the corrugated design. Here, three different gap sizes have been considered (solid curve = 3 mm, dashed = 4 mm and dotted = 5 mm). Only tracks originating from the vicinity of the beam (less than 5 mm) have been considered. The bottom graphs show the results obtained for all

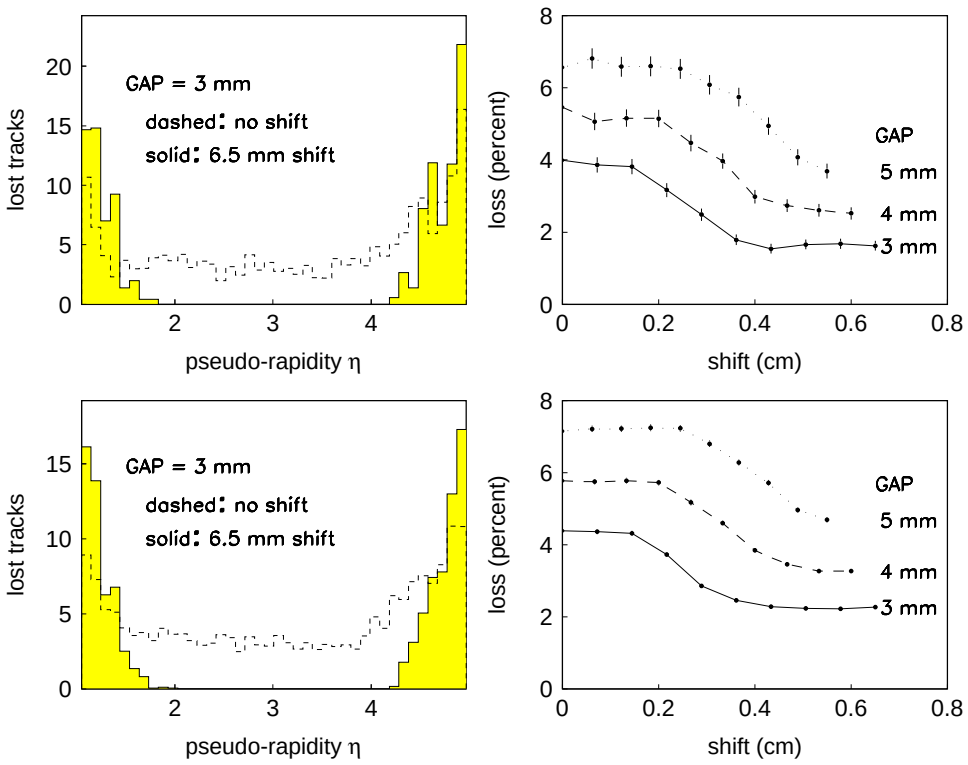

Figure 10: *The figure shows (*left side*) the number of tracks lost due to the acceptance gap as a function of pseudo-rapidity η (solid = 6.5 mm shift, dashed = 0 mm shift). The gap was 3 mm wide. On the (*right side*) the total fractional loss as a function of the gap shift from the mid-plane is plotted for three different gap sizes. Only tracks originating from the vicinity of the beam (less than 5 mm) have been considered.* Top*: tracks from B-meson decay products.* Bottom*: all tracks.*

such tracks, while the top graphs display the results obtained when considering only tracks from B-meson decay products (not only those from $B \to \pi^+\pi^-$). One sees that with a centrally located gap (no shift) the losses are considerable, namely 4 % probability per track, and they are distributed over the whole η range considered here (1 to 5). Shifting maximally the gap away from the mid-plane reduces, as expected, the losses to about 1.5 % probability per track. The losses are concentrated on the edges (small and large η's) of the acceptance. For a physics decay channel requiring n tracks to be reconstructed, this implies an efficiency loss of about $1 - 0.985^n$ (for a gap of 3 mm). For most physics channels we have that $2 \leq n \leq 5$, including tagging, hence the loss of physics events can be expected to be in the range 3 to 7 % depending on the channel.

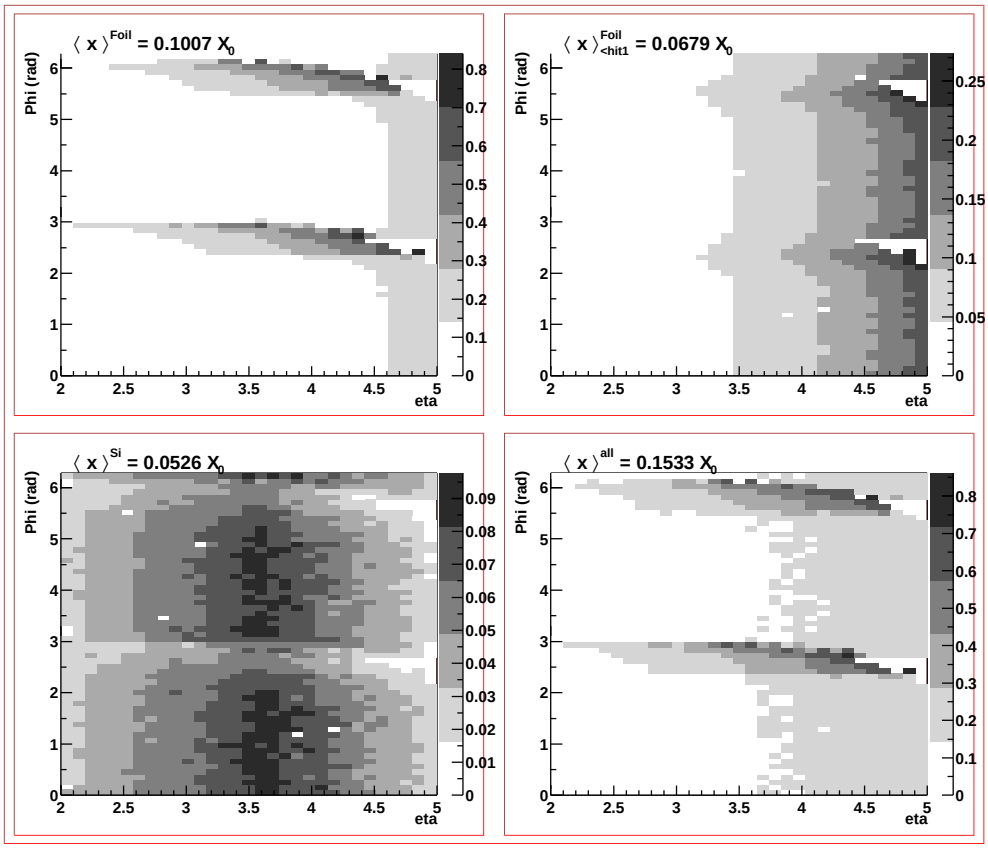

Figure 11: *The figure shows the average amount of material traversed (in radiation lengths) as a function of azimuthal angle 'phi' and pseudo-rapidity 'eta'. See text for a detailed explanation.*

4.1.2 Amount of material seen by particles

The amount of material traversed in the flat foil design (3 mm gap shifted by 6.5 mm, see Fig. 9) was estimated from a stand-alone toy Monte-Carlo simulation in which tracks were generated independently along the z axis with a Gaussian distribution ($\sigma = 5.3$ cm) and flat over the azimuthal angle ϕ and pseudo-rapidity η. The distance traversed in the material is calculated taking into account the impinging angle. For comparing to the corrugated foil design we use results obtained previously [8]. We consider here only the material of the side of the detector vacuum container which is facing the beam (so-called 'topfoil' in Fig. 8) and the material of the silicon sensors.

The plots in Fig. 11 show the average amount of material traversed (in radiation lengths X_0) as a function of azimuthal angle and pseudo-rapidity for a beryllium foil thickness of 1 mm (a realistic thickness, as will be shown in section 4.2). The numbers

can of course be rescaled for any given thickness. The top-left plot shows the contribution of the foil. The dark horizontal bands correspond to a region around the vertical plane where the two foils facing the beam are located. The top-right plot shows the contribution of the foil when considering only the material seen before the first hit on a silicon sensors. The VELO impact parameter resolution is sensitive to this quantity. The bottom-left plot shows, for comparison, the contribution of silicon (with 300 μm thick sensors), while the bottom-right plot gives the sum of the silicon and foil contributions.

	I	II	III
material	**beryllium**	**aluminium**	**aluminium**
geometry	flat foil	flat foil	corrugated
thickness [μm]	1000	250	250
$\langle x/X_0 \rangle_{2.0<\eta<5.0}$	10.0 %	10.0 %	9.3 %
$\langle x/\lambda_I \rangle_{2.0<\eta<5.0}$	8.7 %	2.2 %	2.1 %
$\langle x/X_0 \rangle_{\text{before first hit}}$	6.7 %	6.7 %	3.7 %
$\langle x/X_0 \rangle_{2.0<\eta<4.2}$	7.3 %	7.3 %	8.0 %

Table 2: *Summary of the average amount of RF foil material seen by primary particles. Only the foil facing the beam is taking into account. Column III is derived from Ref. [8]. Column II is obtained by rescaling column I. All numbers are rounded to 0.1 %.*

The results are summarized in table 2. The values in nuclear interaction lengths (λ_I) have been simply obtained by rescaling the X_0 results by λ_I/X_0 for the appropriate material. We also added the results of the flat-foil design for aluminium (250 μm), scaled from the results obtained for beryllium. This allows disentangling to some extent the effects of the material, thickness and geometry. One concludes from this table that, when the flat-foil design is compared to the corrugated-foil design with the same material and thickness, a slight increase (reduction) by a factor 1.1 is obtained in the material traversed, when averaged over the nominal LHCb ('calorimeter') acceptance, namely $2.0 < \eta < 5.0$ ($2.0 < \eta < 4.2$). However, the material traversed before the first hit on a silicon sensor increases by a factor 1.8. The situation is identical when considering a realistic thickness (~ 1 mm) for the beryllium flat-foil design except for $\langle x/\lambda_I \rangle_{2.0<\eta<5.0}$, which is worse for beryllium. All of the improvement due to the material properties is essentially balanced by the increase in thickness. Therefore, our conclusion is that there are no significant advantages with the flat-foil design which suffers from a much reduced stiffness compared to a design with corrugations (see section 4.2 below).

4.2 Mechanical properties of the flat foil design

In order to investigate the feasibility of a low-mass detector vacuum container using flat beryllium foils, FEA calculations have been performed for the design shown in Fig. 8.

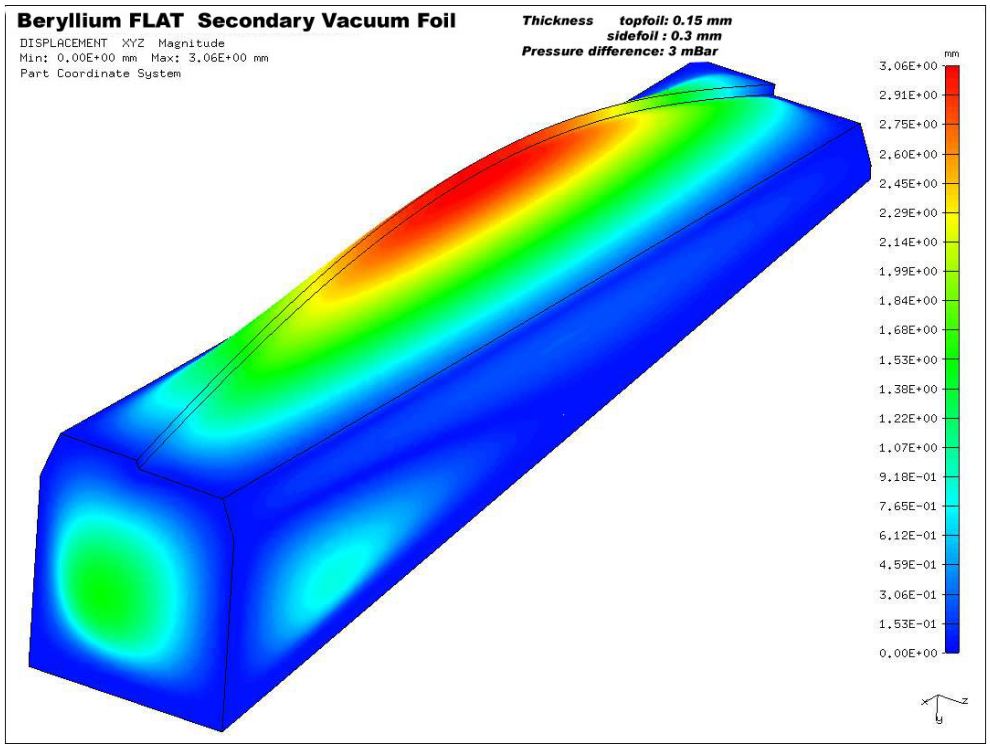

Figure 12: *Deformation of a detector vacuum container made out of beryllium with a flat top foil: only the central part is 0.15 mm thick, the other parts are 0.30 mm. The calculated stresses reached 400 MPa for a 3.2 mbar pressure difference, exceeding the yield strength. The maximal displacement was 3 mm.*

The top foil had a thickness of 0.15 mm, the side foils 0.3 mm. The structure was not stiff enough. At a pressure difference of 2.8 mbar the maximum stress was 400 MPa, exceeding the yield strength of 300 MPa, and the maximum displacement was 4 mm. We have tried to improve the stiffness by changing the top foil thickness to 0.3 mm everywhere but over a width of 110 mm near the 'central' region (beam clearance). The improvement is marginal, as shown in Fig. 12 (the maximum stress was 400 MPa at 3.2 mbar and the maximum displacement was 3 mm).

Figure 13 shows that a 1 mm thick beryllium foil would satisfy our needs for stiffness. The calculated maximum deformation for a 10 mbar pressure difference amounts to 0.23 mm, while the maximum stress is expected to be about 50 MPa, well below the limit of plastic deformation.

The thickness of the foil, however, has a large impact on the material balance. Scaling the values of column I in table 2 shows that a flat foil of 1 mm thickness completely counterbalances the gain obtained from the larger radiation length of beryllium compared to aluminium. Furthermore, in section 4.1 a gap of 3 mm was assumed. More realistically, for a 1 mm thick foil, taking into account the guard ring, the maximum displacement and a safety margin would result in a gap of more than 5 mm. As can be seen from Fig. 10, this would give considerably larger losses of tracks than was estimated at the end of

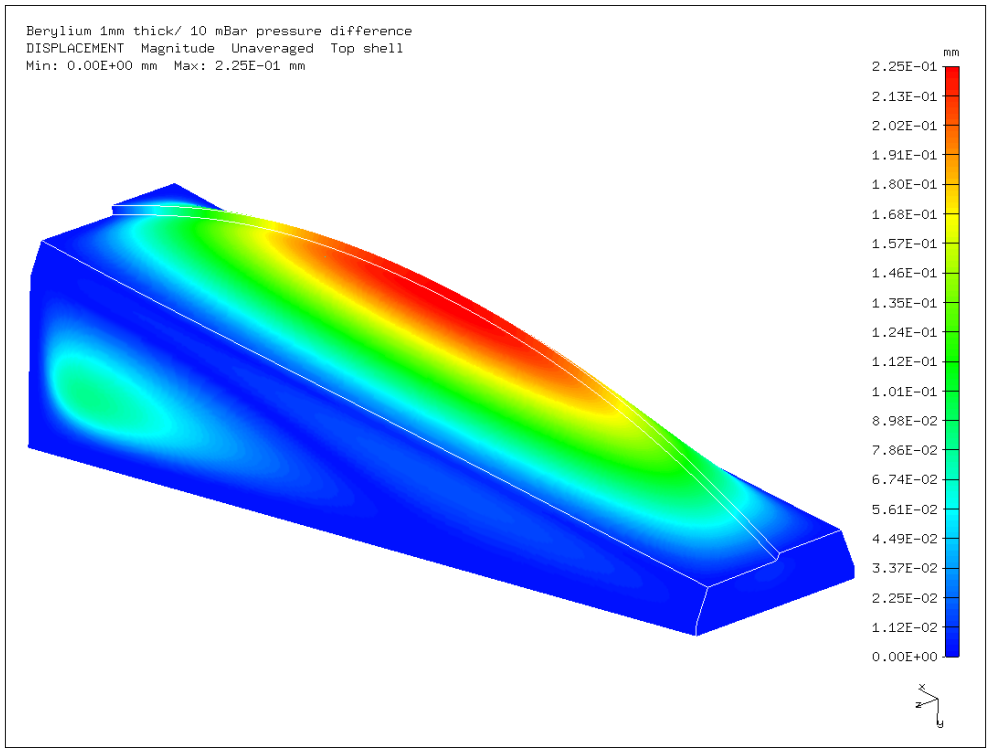

Figure 13: *Deformation of a detector vacuum container made from a 1 mm thick flat beryllium foil for 10 mbar pressure difference. The maximum displacement amounts to 0.23 mm.*

section 4.1.1.

These FEA results, when compared to those presented in section 3, clearly show the beneficial effect of corrugations.

5 Concluding remarks

For a corrugated structure, the excessive high production costs make a design made from beryllium an unrealistic option. We also investigated the use of a design with flat foils. The fact that all corrugations have been removed, dramatically reduces the stiffness of the foil. Consequently, a beryllium thickness of order 1 mm would be needed. This cancels the gain obtained due to the larger radiation length of beryllium compared to aluminium.

Furthermore, such an approach would require a complete redesign of the silicon sensors. Besides that, with a design with a flat foil it is no longer possible to have overlapping sensors. This may result in a substantial loss in the acceptance coverage.

Our conclusion is that a corrugated structure fabricated from AlMg3 remains the most favorable solution.

References

[1] S. Amato *et al.* (LHCb Collaboration), Technical Proposal, CERN-LHCC/1998-4; see also update in *Status of the LHCb Detector Reoptimization*, LHCb Collaboration, CERN-LHCC/2003-003.

[2] S. Amato *et al.* (LHCb Collaboration), Calorimeters Technical Design Report, CERN-LHCC/2000-036.

[3] S. Amato et al. (LHCb Collaboration), RICH Technical Design Report, CERN-LHCC/2000-037.

[4] S. Amato *et al.* (LHCb Collaboration), Muon System Technical Design Report, CERN-LHCC/2001-010.

[5] S. Amato *et al.* (LHCb Collaboration), Vertex Locator Technical Design Report, CERN-LHCC/2001-011.

[6] P.R. Barbosa et al. (LHCb Collaboration), Outer Tracker Technical Design Report, CERN-LHCC/2001-024.

[7] R. Antunes Nobrega *et al.* (LHCb Collaboration), LHCb Technical Design report (Reoptmized Detector Design and Performance), CERN-LHCC/2003-030, chapter 7 and references therein.

[8] J.P. Palacios, LHCb note 2003-072/VELO.